Materials Science in Semiconductor Processing 88 (2018) 173–180

Contents lists available at ScienceDirect

Materials Science in Semiconductor Processing

journal homepage: www.elsevier.com/locate/mssp

Cr doped SnS_2 nanoflowers: Preparation, characterization and photocatalytic decolorization

Wenhua Zhao[a,b], Zhiqiang Wei[a,b,*], Li Zhang[a,b], Xiaojuan Wu[b], Xuan Wang[b]

[a] State Key Laboratory of Advanced Processing and Recycling Nonferrous Metals, Lanzhou University of Technology, Lanzhou 730050, China
[b] School of Science, Lanzhou University of Technology, Lanzhou 730050, China

ARTICLE INFO

Keywords:
Cr doped
SnS_2
Microstructure
Optical
Photocatalytic

ABSTRACT

The $Sn_{1-x}Cr_xS_2$ ($x = 0$, 0.01, 0.03, 0.05 and 0.07) nanoflowers with different molar ratios were prepared via hydrothermal at a low temperature of 180 °C. All samples were characterized by XRD, FT-IR, SEM, EDS, TEM, XPS, UV–vis and PL. The $Sn_{1-x}Cr_xS_2$ nanoflowers are single-phase wurtzite structure with good crystallinity, which is confirmed by the XRD, and FT-IR results. XPS and EDS results demonstrate that Cr is present in the valence of Cr^{3+} ions. Based on the SEM and TEM analysis, the size of doped samples is nearly flower-like ~1.5 µm. The band gap of $Sn_{0.95}Cr_{0.05}S_2$ (2.24 eV) is the largest in the doped samples, which displays the most similar to that of the pure SnS_2 nanoflowers (2.27 eV). The photocatalytic activity of the Cr doped SnS_2 nanoflowers is evaluated towards the decolorization of rhodamine B under visible irradiation with good cyclability and stability. Moreover, the main active species are • OH and h^+. Accordingly, Cr doped SnS_2 displays super photocatalytic performance in dyes decomposition showing the lowest intensity in the PL spectra with doped optimum 5% Cr concentration.

1. Introduction

Facing severe challenges to environmental pollution, it is urgent to develop more novelty photocatalytic materials with the development of human society. There are some advantages of photocatalysis, such as nontoxicity—ideally producing CO_2, H_2O and other nontoxic substances as the final products, high degradation rate, and high efficiency. Diluted magnetic semiconductor (DMS) has the advantages of magnetic materials and semiconductor materials, which has broad application prospects in the fields of optics, magnetism, and photocatalysis in pollutants degradation [1–8]. It has witnessed consequently researches on the semiconductor photocatalytic materials in recent years [9–12].

Owing to its narrow band gap (2.2 eV), low cost, good photoelectric properties, light stability and environmental friendliness, SnS_2 is a suitable candidate for application in photocatalytic degradation of organic pollutant. So far, several succeeding approaches have been made to enhance the efficiency of SnS_2 material for photocatalytic organic dyes degradation [13–16]. Elemental doping generates new energy states within the bandgap of SnS_2, which consists in the intentional incorporation of impurities into the host lattices, is the most commonly used method to tune the optical and chemical properties of nanomaterials. Areej [17] successfully prepared Fe-doped SnS_2 nanosheets using molten salt solid-state reaction and studied its structure and optical properties in detail. Kiruthigaa [18] studied the structural, optical and photocatalytic properties of Ce-doped SnS_2 nanosheets. Wang [19] also observed room temperature ferromagnetism in Mg-doped SnS_2. Chen [20] studied the photocatalytic activity of Ni-modified chromium-reduced SnS_2 nanosheets under visible light irradiation. Park [21] similarly studied the photocatalytic performance of In-doped flower-like SnS_2. An [22] also synthesized a graphene oxide-doped SnS_2 nanosheet with enhanced visible light photocatalytic activity to reduce the graphene oxide junction by means of biomolecular assisted preparation.

Recently, Cr-doped SnS_2 nanoflowers were found to be efficient for visible-light driven photocatalysis in two reasons. First, the doping enhances the absorption in the visible region. Second, the new energy states efficiently promote the separation of photogenerated electron-hole pair resulting in more photo-generated charges participating in photocatalytic reaction. However, up to now, no report has been made about optical properties and photocatalytic properties of Cr^{3+} doped SnS_2 nanomaterials, especially.

In this paper, pure SnS_2 and $Sn_{1-x}Cr_xS_2$ ($x = 0.01$, 0.03, 0.05 and 0.07) nanoflowers were successfully prepared via a hydrothermal method using triton as a surface modifier. The samples were characterized by XRD, FTIR, XPS, SEM, HRTEM, UV–vis, EDS and PL to

---

* Corresponding author at: State Key Laboratory of Advanced Processing and Recycling Nonferrous Metals, Lanzhou University of Technology, Lanzhou 730050, China.

E-mail address: qianweizuo@163.com (Z. Wei).

https://doi.org/10.1016/j.mssp.2018.08.011
Received 15 May 2018; Received in revised form 17 July 2018; Accepted 11 August 2018

comprehensively analyze the microstructure, morphology, elemental content, optical and photocatalytic properties. In addition, the as-prepared $Sn_{1-x}Cr_xS_2$ ($x = 0$, 0.01, 0.03, 0.05 and 0.07) nanoflowers exhibit an obvious enhancement of photocatalytic activities for decolorization of Rhodamine B (RhB) aqueous solution under simulated sunlight irradiation compared to pure SnS_2, which was mainly ascribed to the new energy states restrain the generation of photogenerated electrons - hole pairs.

2. Material and methods

2.1. Synthesis of the $Sn_{1-x}Cr_xS_2$ nanoflowers

Pure SnS_2 and $Sn_{1-x}Cr_xS_2$ (x = 0.01, 0.03, 0.05 and 0.07) nanocrystals were prepared by hydrothermal method. All raw materials used in this study were analytical grade and used without further purification. The manufacturing process was as follows: The tin chloride ($SnCl_4·5H_2O$), chrome chloride ($CrCl_3·6H_2O$) and thiourea ($(NH_2)_2CS$) were weighed stoichiometric according to the chemical formula and the mole ratio of the metal cation of $Sn_{1-x}Cr_xS_2$. Then mixed materials were dissolved in 5 mL Triton X-100 and 65 mL of deionized water to obtain a solution, magnetically stirred at room temperature for 30 min. Finally, the resulting mixed solution was transferred into a 100 mL Teflon lined stainless steel autoclave, the hydrothermal synthesis heated at 180 °C for 18 h in an oven. The resulting precipitates were thoroughly washed with deionized water and absolute alcohol several times by centrifugation to remove impurities. The obtained products were dried in an oven at 60 °C for 12 h. Thus, $Sn_{1-x}Cr_xS_2$ (x = 0, 0.01, 0.03, 0.05 and 0.07) nanocrystals were collected and used for further studies.

2.2. Characterization

The phase and structural analysis of as synthesized samples were examined by a powder X-ray diffractometer (Japan Rigaku D/Max-2400) with CuKa radiation at $\lambda = 1.54056$ Å. The flourier transform infrared spectrum of the sample was measured by infrared spectrometer (Nexus 670). The X-ray photoelectron spectroscopy (Bestec, Germany) measurements were performed to study the chemical states of the elements. The morphology and microstructure of the samples were observed by field emission scanning electron microscope (FESEM, 200FEG) and high-resolution transmission electron microscopy (JEM-2010). The optical properties were analyzed using ultraviolet-visible (TU-1901) spectrophotometer. Photoluminescence spectra were recorded on a PerkinElmer fluorescence spectrometer with the excitation wavelength of 300 nm.

2.3. Measurement of photocatalytic activity

The photocatalytic abilities of $Sn_{1-x}Cr_xS_2$ ($x = 0$, 0.01, 0.03, 0.05 and 0.07) were investigated via the photocatalytic decolorization of Rhodamine B (RhB) under visible light irradiation at room temperature. A 300 W xenon lamp was used as the simulated sunlight source to evaluate the photocatalytic activity of the samples. In a typical process, 50 mg of catalyst was added to 100 mL of RhB aqueous solution ($C_0 = 10$ mg/L). The mixed suspensions were magnetically stirred in the dark for 30 min to ensure the adsorption-desorption equilibrium of the prepared catalysts and organic dye molecules, obtaining the colloidal solution. Equipped with a magnetic stirrer under visible light positioned horizontally, the photocatalytic experiment was conducted at room temperature in a cylindrical glass vessel with 30 cm above the colloid surface. At the regular time intervals, approximately 3 mL of the irradiated suspensions was extracted and centrifuged to remove the catalyst. The supernatant after centrifuging was recorded to observe the adsorption and decolorization performance. In the direction of assessing the degree of decolorization of organic pollutant, the typical absorption peak of RhB at 554 nm was chosen as a reference point in absorption spectra. The photocatalytic decolorization efficiency is defined by the following equation: $\eta = (C_0 - C_t)/C_0 \times 100\%$, where C_0 is the initial concentration of RhB and C_t means the concentration of RhB after light irradiation.

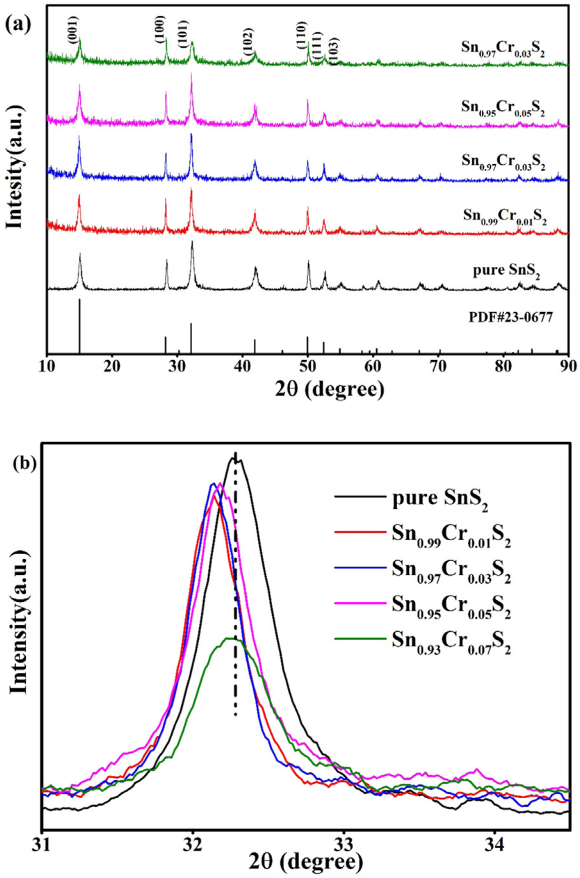

Fig. 1. Pure SnS_2 and $Sn_{1-x}Cr_xS_2$nanoflowers (a) XRD; (b) Magnification of (101) peak.

The $Sn_{1-x}Cr_xS_2$ samples were weighed 0.5 g to add into 100 mL RhB at an initial concentration of 5 mg/L. Different capture agents, such as sodium sulfate, triethanolamine, isopropanol were added to the organic dye, respectively. Then, the above photocatalysis experiment is repeated.

3. Results and discussion

3.1. Structure analysis

The XRD patterns of different doping concentrations of $Sn_{1-x}Cr_xS_2$ (x = 0, 0.01, 0.03, 0.05 and 0.07) samples are shown in Fig. 1. The locations and relative intensities of the diffraction peaks are basically the same as those of the SnS_2 standard card JCPDS (23-0677), it is indicated that the sample belongs to the hexagonal wurtzite crystal structure. The XRD pattern does not show the second-phase diffraction peaks of Cr metal clusters and other chromium sulfides. When $x < 0.07$, metal doped in semiconductor lattice makes the slight shift to lower scattering angles from the magnified image of (101) peak in Fig. 1(b). Meanwhile, it can be seen from Table 1 that the lattice constants and inter-planar spacing of Cr doped samples are greater than that of pure SnS_2 because that the ion radius of Cr^{3+} is smaller than of Sn^{4+}. When the doping concentration increases up to $x = 0.07$, the lattice constant, cell volume and inter-planar spacing of the samples decrease. It turns out that the metal ion Cr^{3+} is doped into the SnS_2